JOURNAL OF GEOPHYSICLA RESEARCH, VOL. 86, NO. A9, PAGES 7639-7648, SEPTEMBER 1, 1981

DEPENDENCE OF POLAR CAP POTENTIAL DROP ON INTERPLANETARY PARAMETERS

P. H. Reiff, R. W. Spiro, and T. W. Hill

Space Physics and Astronomy Department, Rice University, Houston, Texas 77001

Abstract. We have computed the convection potential drop across the polar cap from data obtained on high-inclination low-altitude satellites (AE-C, AE-D, S3-3) and correlated these potential measurements with various combinations of parameters measured simultaneously in the upstream solar wind. These combinations of solar wind parameters consist of predictions based on magnetic merging theory and suggestions based on earlier empirical work. We find that the bulk of the potential drop, and its variation with interplanetary magnetic field (IMF) parameters, are successfully predicted by merging theory (to the accuracy with which they can presently be measured), but that a significant 'background' potential drop (~ 35 kV) does not depend on IMF parameters and may thus be attributed to an unknown process other than merging. Our results indicate that small values of the IMF are amplified by a factor of 5-10 at the dayside magnetopause as a combined effect of bow shock compression and the Zwan-Wolf depletion layer effect; correlations between IMF parameters and the polar cap potential drop are dramatically improved when this amplification is taken into account. The potential drop is better correlated with IMF parameters than with geomagnetic activity indices, presumably because the latter are affected by nonlinear reponses of the magnetosphere to the polar cap input.

Introduction

The electric potential drop across the earth's polar cap is a direct measure of the rate of plasma flow through the magnetospheric convection system. The polar cap is defined for our purposes as the region of generally anti-sunward convection that is always found to exist in the high-latitude ionosphere (see, for example, the review by Stern [1977] and references cited therein). The antisunward convection is driven ultimately by the solar wind, and the polar cap potential drop is thus a potentially useful indicator of the instantaneous strength of solar wind/magnetosphere coupling. It is also an essential input parameter for quantitative modeling studies of the dynamics of the inner magnetosphere and sub-auroral ionosphere (see, for example, Wolf [1970] and Harel et al. [1981] and references therein). The dependence of the polar cap potential drop on interplanetary parameters is thus a question of both theoretical and practical significance.

Several empirical studies have established the existence of a strong correlation between east-west asymmetries in the polar cap convection pattern and the east-west component of the interplanetary magnetic field (IMF) (see, for example, the reviews by Burch [1974], Stern [1977], and Cowley [1981], and references therein). This correlation is most easily explained in terms of the open magnetosphere model [Dungey, 1961], in which the polar cap convection is driven by magnetic stress transmitted along 'open' or 'interconnected' magnetic field lines connecting the geomagnetic and interplanetary magnetic fields (see, for example, the discussion by Russell and Atkinson [1973]). Another unavoidable prediction of the open-model hypothesis is that the total strength of the convection system, as measured by the polar cap potential drop, should be an increasing function of the southward component of the IMF, this component being most favorable for the 'merging' process whereby geomagnetic flux becomes interconnected with interplanetary flux on the dayside magnetopause. To our knowledge, this prediction has never been directly tested, and such a test is the primary purpose of this paper. (A lack of such correlation was tentatively reported by Heppner [1972] on the basis of the very limited data set then available.)

Several studies have shown a strong positive correlation between the southward IMF component and a variety of geomagnetic and auroral activity indices [e.g., Arnoldy, 1971; Foster et al., 1971; Rostoker et al., 1972; Murayama and Hakamada, 1975; Garrett et al., 1974; Burch, 1974]. In view of the widespread belief that magnetospheric convection powers most of the geomagnetic disturbances that are reflected in the activity indices, it is plausible (and perhaps customary), but by no means logically necessary, to infer from these studies that the polar cap potential drop is itself correlated with the southward IMF component. Only recently have the appropriate satellite data become available to perform a statistical corelation analysis directly between the polar cap potential drop and simultaneous solar wind parameters including, but not limited to, the southward IMF component.

Before proceeding to the data analysis we give a capsule summary of the theoretical motivations for the study.

Expectations

Several theoretical arguments have dealt specifically with the dependence on interplanetary parameters of the dayside merging rate and hence (within the open model) the cross polar cap potential drop [e.g., Petschek, 1966; Gonzales and Mozer, 1974; Sonnerup, 1974; Hill, 1975; Crooker, 1979]. For example, Hill [1975] calculated the dissipative component of the electric field $\underline{E}$ (i.e., its component E_j parallel to the magnetopause current $\underline{J}$) for a plane magnetopause model separating external field $\underline{B}_1$ and internal field $\underline{B}_2$. The results are summarized in Figure 1, a normalized plot of E_j versus θ, the angle between $\underline{B}_1$ and $\underline{B}_2$, for two values of the ratio $\alpha = B_1/B_2$. The solid and dashed curves follow from different possible assumptions regarding the dependence of the merging rate on

Paper number 1A1042.
0148-0227/81/001A-1042$01.00

field orientation: the solid curve is appropriate if the merging rate is independent of field orientation, while the dashed curve is appropriate if the merging rate is proportional to the component of $\underline{B}_1$ antiparallel to $\underline{B}_2$. (The merging rate is defined, following Vasyliunas [1975], as the ratio of the magnetosheath flow component normal to the magnetopause v_n to the magnetosheath Alfvén speed v_A, or, equivalently [Hill, 1975], the ratio of the field component B_n normal to the magnetopause to the external field strength B_1.) The former case (solid curves) is represented by

$$E_j/E_o = \alpha^2(\alpha - \cos\theta)/(1 + \alpha^2 - 2\alpha\cos\theta)^{1/2} \quad (1)$$

(equation (62) of Hill [1975]), and the latter case (dashed curves) by

$$E_j/E_o = \alpha^2(\alpha - \cos\theta)^2/(1 + \alpha^2 - 2\alpha\cos\theta) \quad (2)$$

(equation (65) of Hill [1975]), with

$$E_o \equiv (B_2^2/\sqrt{\mu_o\rho_1})(B_n/B_1) \quad (3)$$

where ρ_1 is the mass density outside the magnetopause.

One can make topological arguments [e.g., Gonzales and Mozer, 1974; Sonnerup, 1974] to the effect that the direction of the magnetopause current $\underline{J}$ defines a symmetry axis of the merging flow geometry (the 'merging line'), and from this it follows geometrically that the potential drop ϕ across the merging region is proportional to E_j as given by (1) or (2) above, given that the geometry of the merging region is otherwise symmetric about the earth-sun line (see, however, Cowley [1976]). (The length of the merging line, i.e., the ratio of ϕ to E_j, may itself be a function of θ (see, e.g., Atkinson [1978]), but any such dependence is likely to be weak, and the form of the dependence is not well established theoretically, so we will assume here that $\phi \propto E_j$ except in those cases where a particular theory specifies otherwise.) Barring large, systematic, magnetic-field-aligned potential drops, one would then expect the cross polar cap potential drop (to the extent that it depends on dayside magnetic merging) to respond to interplanetary parameters somewhat as specified by (1) or (2) above.

Through a similar argument, Sonnerup [1974] had previously arrived at equation (2) above. Gonzales and Mozer [1974], through purely geometrical arguments, arrived at an angular dependence similar to that of equation (1) above. Petschek [1966] had earlier proposed a dependence $\sin(\theta/2)$ for the merging rate, which would imply a dependence $\sin^2(\theta/2)$ for the potential drop [Sonnerup, 1974]; this represents (2) in the limit $\alpha = 1$. Crooker [1979] has proposed that the merging rate is significant only for local values of θ very near 180°, but that a locus of points with $\theta \approx 180°$ can be found near the polar cusp region of the magnetopause for any orientation of the IMF. Topological considerations then favor the establishment of a large convection potential drop when the IMF is large and southward. Although no explicit dependence on IMF parameters has been derived from such a model, the qualitative dependence described by Crooker [1979] is similar to that shown in Figure 1.

We thus adopt (1) and/or (2) as representative of expectations based upon a rather general class of magnetic merging theories. It should be noted that α and θ in (1) and (2) refer to the magnetic field immediately outside the subsolar magnetopause, and one must be careful to relate this field in the proper way to the upstream (preshock) IMF which is the actual measured quantity. We shall return to this problem in the procedure section below.

Kan and Lee [1979] have presented a modification of the above merging theories in which they derive the result

$$\phi \propto vB \sin^2(\theta/2) \quad (4)$$

This derivation relies on the following three assumptions: (1) the merging electric field is represented by $E_j = v_1B_1\sin(\theta/2)$, which is the $\alpha = 1$ limit of equation (1) above, multiplied by v_1B_1; (2) the component E_j is assumed to be continuous across the magnetopause, but the other tangential component of $\underline{E}$ is assumed to be zero inside the magnetopause; and (3) the total magnetosheath electric field v_1B_1 is set equal to its solar-wind value vB. Although we do not understand the justification for any of these assumptions, we shall include equation (4) among the theoretical predictions tested.

It has also been proposed that, within a closed model of the magnetosphere, anti-sunward convection may be driven either by anomalous (non-collisional) viscosity at the magnetopause [Axford and Hines, 1961] or by pressure gradient forces on magnetosheath plasma that 'somehow' diffuses across the dayside magnetopause [Johnson, 1978]. Theoretical treatments of such closed model transfer processes are lacking, and it is not clear how, or if, the efficiency of such processes should depend on the IMF and solar wind parameters. Preliminary calculations [Eviatar and Wolf, 1968; Hill and Wolf, 1977; Hill, 1979] suggest that a potential drop of ~ 10 kV may be established by the viscosity associated with rapid cross-field diffusion, independent of the IMF orientation. We shall tentatively attribute to closed model processes any residual potential drop that occurs for nearly northward IMF when the open model predicts zero, e.g., when $\cos\theta > \alpha$ in (1) and (2) above.

In addition to the theoretical work cited above, numerous combinations of solar wind and IMF parameters have been found empirically to correlate strongly with geomagnetic activity. Representative examples are B_s [Arnoldy, 1971], vB_s [Rostoker et al., 1972], and $\varepsilon = vB^2\sin^4(\theta/2)$ [Perreault and Akasofu, 1978], where v is solar wind velocity, B is IMF magnitude, θ is the angle between the IMF and the (northward) z axis of a solar magnetospheric coordinate system, and $B_s = -B_z$ when B_z is negative and $B_s = 0$ when B_z is positive. Although the theoretical motivation for these expressions is not clear, we shall include them (and others) in our correlation analysis for the sake of completeness.

Procedure

Orbit Selection Criteria

The AE-C satellite orbited over 25,000 times before it decayed; the AE-D satellite, over 1400

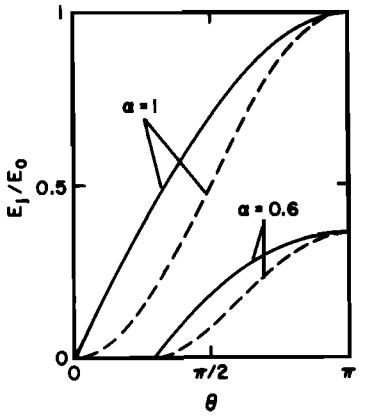

Fig. 1. Theoretical dependence of the polar cap potential drop on the angle θ between the fields B_1 (outside the dayside magnetopause) and B_2 (inside the magnetopause), for two values of $\alpha = B_1/B_2$. The solid curves (equation (1) of the text) result from the assumption that the merging speed is independent of θ, while the dashed curves (equation (2) of the text) result from the assumption that the merging speed is proportional to the component of B_1 antiparallel to B_2 [Sonnerup, 1974; Hill, 1975].

times. Every orbit track was examined in order to determine which passes were oriented sufficiently in the dawn-to-dusk direction for this study. The following preliminary criteria were established: the orbit must have crossed the 60° invariant latitude curve within three hours of both dawn and dusk: i.e., between 0300 and 0900 magnetic local time (MLT) and again between 1500 and 2100 MLT. In addition, we required that the satellite reached a maximum invariant latitude of at least 75° if on the night side and at least 78° if on the dayside. Finally, we required that the satellite was in the despun mode (one revolution per orbit), in order to have the highest resolution of ion drift meter (DM) and retarding potential analyzer (RPA) data. These data were provided through the AE Computer System by courtesy of the principal investigator, W. B. Hanson, and are described in detail by Hanson et al. [1973].

Several hundred orbits satisfied these preliminary criteria. Next we examined microfilm plots of the DM data in order to check whether the spacecraft was taking data in an appropriate mode over the complete polar cap pass (defined here as the region of anti-sunward convection from reversal to reversal), without serious data gaps. Next we examined microfilm plots of the geocentric solar ecliptic (SE) components of the IMF from IMP-J, courtesy of N. F. Ness and the World Data Center. A preliminary study using 40-min averages of these SE data was reported by Reiff et al. [1979].

The potential drops were calculated for those orbits for which IMF data were available, and we corrected these values for satellite pointing errors (see below). We then generated polar plots of the measured convection velocities and re-examined our selection criteria. We tightened our criteria to require that the polar cap boundary (defined by the extrema in corrected potential in case of multiple electric field reversals) was crossed within 3 hours of dawn-dusk MLT. Because the auroral oval is known to be offset from the magnetic pole toward midnight [Feldstein, 1973; Meng et al., 1977], we shifted our 'dawn-dusk' line 3.5° toward midnight. This had the effect of eliminating all dayside passes of AE-C, whose inclination was only 68°.

Because the polar cap is smaller when the IMF is northward [e.g., Burch, 1973], and because of the 68° inclination of the AE-C orbit, our selection criteria generally tended to favor orbits when the IMF was southward. This has the effect of eliminating most of the cases of strong reversed (sunward) polar cap convection [Burke et al., 1979] because these generally occur when the IMF is northward [Spiro et al., 1979]. Of the 32 orbits finally selected, nine had $B_z > 0$ (in SM coordinates), and 23 had $B_z < 0$. Polar plots of these 32 orbits are shown in Figure 2.

Data Analysis

The DM and RPA measurements of the ionospheric flow velocity were combined with the International Geomagnetic Reference Field to yield the electric field component along the spacecraft trajectory (the corotation field was subtracted).

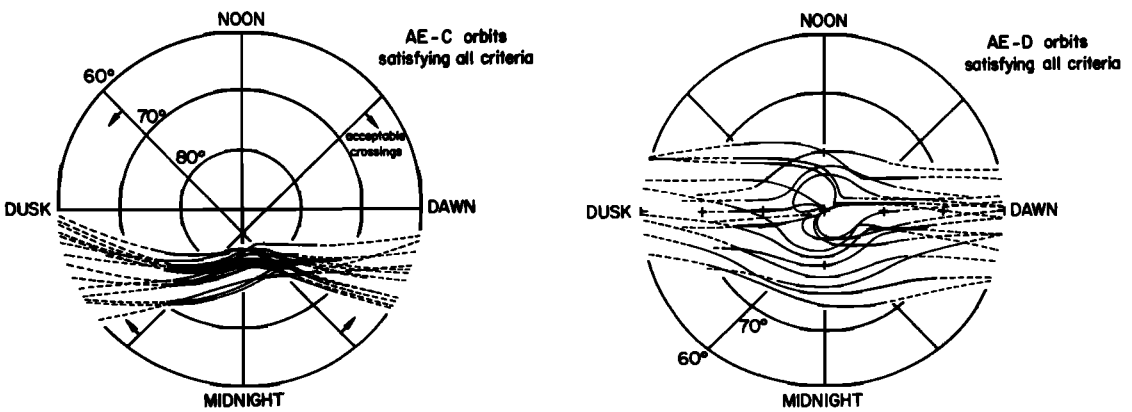

Fig. 2. The 32 AE-C (a) and AE-D (b) orbits used in this study are plotted in invariant latitude (Λ) and magnetic local time (MLT) coordinates. The solid portion of each trajectory lies within the polar cap.

The electric potential was then calculated as a function of distance along the trajectory, and the cross polar cap potential drop was defined as the difference between the dawnside potential maximum and the duskside potential minimum.

Multiple electric field reversals occurred on most of the orbits, most frequently within the plasma sheet (i.e., the region of sunward convective flow equatorward of the dawn and duskside potential extrema), where they are associated with inverted V electron precipitation structures. The effect of these minor reversals is minimized in our calculation of the potential drop by taking the potential extrema (rather than the most equatorward electric field reversals) as the polar cap boundaries (see Fig. 3). Thus, our polar cap potential drop represents the maximum range of variation of the electric potential during the polar crossing.

Several orbits showed evidence of reversed (sunward) convection within the polar cap (e.g., Burke et al. [1979]). Such reverse convection cells, being contained within the polar cap, contribute no net potential difference to the total cross polar cap potential drop; they may, however, present some difficulty in our scheme for determining the polar-cap boundaries from the potential extrema. Figure 3 illustrates the case of a single imbedded reverse convection cell [Crooker, 1979] near the dawnside polar cap boundary. In this case, if the potential variation within the imbedded cell ($\phi_B - \phi_C$) exceeds that within the adjacent boundary layer cell ($\phi_D - \phi_C$), then the dawnside potential maximum (ϕ_B) occurs poleward of the actual polar cap boundary (D), and we overestimate the true cross polar cap potential drop (we obtain $\phi_B - \phi_A$ rather than the actual value $\phi_D - \phi_A$). We have examined all of the AE orbits used in this study, and we conclude that we overestimate the potential drop by at most ~ 5 kV in such cases. Thus, although imbedded reverse convection cells are present in several of our orbits, their presence does not seriously affect our determination of the polar cap potential drop.

Minor uncertainties in the orientation of the satellite can cause baseline errors in the calculated electric field, and thus errors in the derived potential difference. A 1° pointing error at a vehicle speed of 8 km/s can cause a baseline electric field error of 7 mV/m (up to 24 kV error for a polar cap of radius 15°). Pointing errors can be detected in two ways: (1) the electric field should decrease to zero at low latitudes because the Alfvén layer shields the inner magnetosphere from convection [e.g., Wolf, 1970]; (2) for steady state conditions, the potential across the polar cap should be exactly balanced by the sum of potentials across the dawn and dusk plasma sheets (i.e., the regions of sunward convective flow). An imbalance may be attributed to pointing errors [Banks et al., 1981]. (However, some residual imbalance may be real and attributable to magnetic flux buildup in the tail during substorm growth phases [Caan et al., 1975], or to time variations of the potential pattern occurring as the satellite crosses the polar cap (~ 15 min).)

In practice, therefore, we integrated the potential from invariant latitude $\Lambda = 50°$ on the duskside across the pole to $\Lambda = 50°$ on the dawnside. We took any residual potential difference, divided it by the distance travelled, and calculated the offset electric field. We checked the offset electric field against the residual electric field at low latitudes. If they agreed, the potential was recomputed by subtracting the inferred offset. If they disagreed, or if the data from one or the other plasma sheet were incomplete, an offset was calculated from the low-latitude electric field value (only three orbits had offsets larger than 5 mV/m). We estimate that the potentials reported here are accurate at least to within ± 20 kV, and probably better. Since the data range from 30 kV to 140 kV (with a mean value 70 kV), this inaccuracy is not too damaging. (The highest potential measured, 175 kV, had to be discarded because IMF data were not available.)

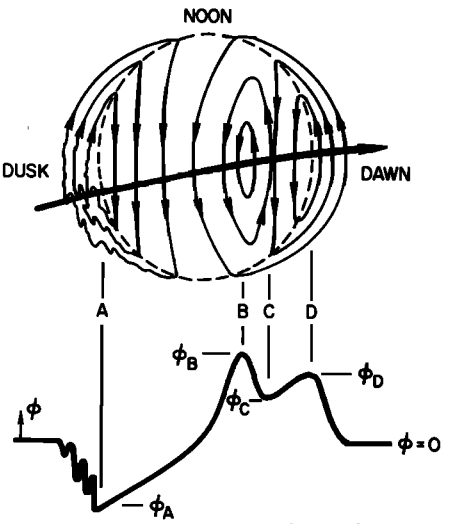

Fig. 3. A sketch of a possible polar cap convection pattern, illustrating possible ambiguities in determining the cross polar cap potential drop. The dashed line represents the polar cap boundary, i.e., the primary transition between sunward and antisunward convection in the overall flow pattern. A hypothetical satellite trajectory is represented by the heavy line crossing the polar cap from dusk to dawn, and the hypothetically measured variation of electric potential along that trajectory is represented by the heavy curve below. In the duskside plasma sheet (to the left of point A), multiple electric field reversals are associated with inverted-V electron precipitation structures; the effect of these reversals is eliminated by taking the polar cap boundary to be located at the position (A) of the duskside potential minimum (ϕ_A), rather than at the most equatorward electric field reversal. The dawnside of the polar cap in this example contains an imbedded reverse convection cell (between B and C). If $\phi_B > \phi_D$, as illustrated here, then our procedure would be in error—we would place the boundary at (B) rather than its actual location (D). We would thus overestimate the cross polar cap potential drop as ($\phi_B - \phi_A$) compared to its actual value ($\phi_D - \phi_A$). Examination of all orbits considered in this study indicates that the magnitude of such overestimates is, at most, about 5 kV.

Interplanetary Data

Hourly values of the GSM components of the IMF and the solar wind velocity were obtained from the Interplanetary Medium Data Book [King, 1979]. The bulk of the data were from the satellite IMP-J; however, others were used as available. (The SE system was tested and found to yield smaller correlation coefficients than the SM system, in agreement with Russell and McPherron [1973]; therefore, only SM data are used here.)

It is well known that the Auroral Electrojet index (AE) responds to IMF changes with about a one-hour time lag [e.g., Arnoldy, 1971; Garrett et al., 1974]. It is likely, however, that the polar cap potential responds more directly, and hence more quickly, to changes in the IMF than does the AE index. After a limited amount of optimization testing, we found the following scheme to yield the highest correlations: if the orbit culminated (reached its highest invariant latitude) during the last thirty-five minutes of a particular hour (UT), the IMF data for that hour were used. If the orbit culminated in the first twenty-five minutes of the hour, the previous hour's IMF data were used. Obviously, this lag could be reoptimized for each of the functions tested, but this has not been done.

Other parameters tested (AE, Kp) were calculated with no time lag; i.e., the parameters were used from the hour in which the satellite orbit culminated.

S3-3 Orbits

It became apparent that potentials measured when the IMF magnitude was large ($|B| > 15$ nT) were smaller than would be expected from linear extrapolation of the results obtained from low-field values only. We interpret this effect as being due to large amplifications of the magnetosheath magnetic field strength compared to the solar wind field (roughly by a factor of eight). This amplification is limited, however, such that the magnetosheath field strength does not exceed that of the internal geomagnetic field (see below).

To quantify this amplification/limitation process required as many orbits as possible during times of large IMF magnitude. Only two AE orbits occurred with $|B| > 15$ nT; to improve the statistics we have included three orbits of data from the S3-3 satellite taken when $|B| > 15$ nT (thus increasing the total number of orbits to 35). These passes were part of the CDAW 2.1 workshop; the S3-3 electric field data are provided by F. S. Mozer and the IMP-J magnetic field data by N. F. Ness. During two of these passes, the electric field instrument saturated and therefore gives only lower limits to the potential. The low-altitude potential drop may, in any case, be reduced somewhat in comparison with the high-altitude value as the result of magnetic-field-aligned potential differences. No corrections were applied to the S3-3 potentials.

Amplification and Limitation of the IMF

In (1) and (2) above, and in equations (14) and (16) of Gonzales and Mozer [1974], the field B_1 refers explicitly to the field in the magnetosheath, just outside the nose of the magnetopause. In MHD calculations [Spreiter and Alksne, 1969] the ratio of magnetosheath nose particle density to solar wind density is 4.2 (somewhat dependent on the choice of solar wind mach number and adiabatic index). In those models the field strength scales linearly with the particle density.

As the field is compressed against the magnetopause, the plasma has a tendency to escape along field lines, enhancing the nose ratio of field strength to plasma density by perhaps a factor of 2 [Zwan and Wolf, 1976]. This effect has been observed in the subsolar magnetosheath [Crooker, 1977]. Thus, amplification of the magnetosheath field strength over the solar wind field strength by factors of up to eight are plausible.

On the other hand, amplifying a 30 nT interplanetary field by a factor of eight would imply a sheath field of 240 nT, four times larger than the typical internal field strength. It is obvious from pressure balance considerations that the sheath field strength should rarely, if ever, exceed the internal field strength. (Large IMF magnitudes are likely associated with small solar wind magnetosonic mach numbers and hence small shock compression ratios.) Therefore, in testing (1) and (2) against the observed potential drops, we have used $\alpha = fB_{sw}/60$ nT, where f is an amplification factor to be optimized from the empirical fits. If the resulting value of α exceeded unity, it was replaced by $\alpha = 1$, i.e., the condition $B_1 \leq B_2$ was imposed. Note that this limiting procedure is different from that used by Gonzales and Mozer [1974]: When 5 B_{sw} exceeded the internal field (taken there to be 70 nT), they set the entire function, rather than α, equal to unity. This has the effect of making their predictions for large northward IMF much larger than the observed values. On the other hand, limiting α as we have done retains the angular information in (1) and (2). Like Gonzales and Mozer, we also set the function equal to zero when $\alpha - \cos\theta < 0$.

Atkinson [1978] has simulated this compression/depletion effect by means of a simple hydrodynamic model of magnetosheath flow that incorporates, in an approximate way, the merging theory results cited above. He utilizes two angular dependences $E_j(\theta)$ that correspond to the $\alpha = 0$ and $\alpha = 1$ limits of (1) above, and also prescribes a formula for the θ-dependence of the width of the merging region. In testing his model result for ϕ as a function of interplanetary parameters, we have not employed the amplification/limitation procedure because this effect is explicitly included (in a different way) in his model. Likewise, the model of Kan and Lee [1979] gives ϕ as an explicit function of upstream solar wind parameters, so the amplification/limitation procedure is not applied to their result either.

Gonzales and Mozer [1974] and Atkinson [1978] also specified that in their results only the transverse components of the IMF (in the y_{SM}-z_{SM} plane) should be used to calculate the incident IMF magnitude, presumably because only those components are compressed at the subsolar point of the bow shock. Because of the complicated three-dimensional geometry of the magnetosheath magne-

tic field, however, all three components of the IMF are subject to some shock compression, and all three components in general contribute to the field just outside the dayside magnetopause. Lacking any clear cut theoretical preference, we have done each of the correlation analyses in two ways, one using the total IMF field strength and the other using only its y_{SM} and z_{SM} components. We found no systematic difference in the results of these two procedures, and the correlations presented below are all obtained from the first procedure (total IMF strength), except for the Gonzales/Mozer and Atkinson functions where the results of the second procedure are shown, that procedure having been explicitly prescribed by those authors.

The same amplification/limitation procedure was applied to all interplanetary functions tested (with the exceptions of the Atkinson [1978] and Kan and Lee [1979] functions as noted above), i.e., B_{sw} was replaced by the smaller of B_{sw} or (60nT)/f and the value of f was optimized for each function individually. For those functions involving a component of the IMF, e.g., B_z, the component B_z was multiplied by the ratio (60 nT)/(fB_{sw}) whenever that ratio was less than unity. The angle θ was not changed by this procedure.

Results

The degree of correlation between interplanetary parameters and the polar cap potential drop turns out to be quite sensitive to the way in

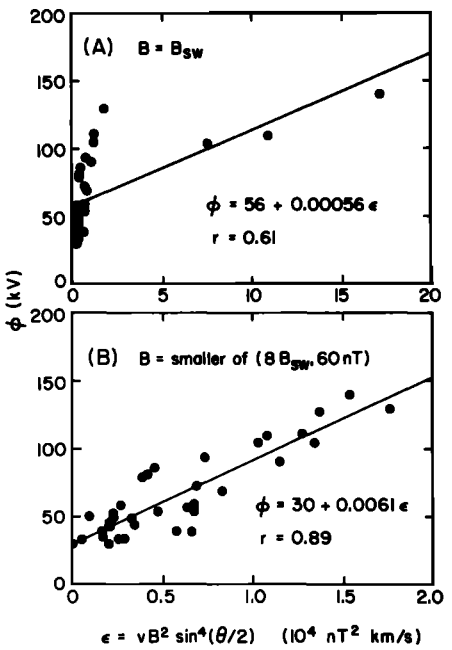

Fig. 4. Observed polar-cap potential drop ϕ versus the Perrault-Akasofu parameter $\epsilon = vB^2\sin^4(\theta/2)$. In (a), the parameter B is set equal to the IMF strength, while in (b) it is derived from the IMF by the amplification/limitation procedure described in the text. The straight lines are the least-squares fits to the data, with correlation coefficients r = 0.61 in case (a) versus r = 0.89 in case (b). (Note the factor-of-ten difference in horizontal scales.)

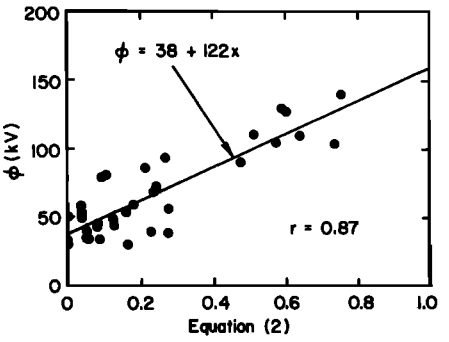

Fig. 5. Observed polar cap potential drop ϕ versus E_j/E_0 from the right-hand side of equation (2) of the text (a prediction based on magnetic merging theory). The best-fit straight line, as shown, has a correlation coefficient r = 0.87.

which the magnetosheath field $\underline{B}_1$ is inferred from the (observed) solar wind field $\underline{B}_{sw}$. This dependence is illustrated in Figure 4 where the potential drop ϕ is plotted against two versions of the Perrault-Akasofu parameter $\epsilon = vB^2\sin^4(\theta/2)$. When B in this expression is taken as B_{sw}, a correlation coefficient of only 0.61 results (Figure 4a), whereas the correlation coefficient increases to an impressive 0.89 when B is modified by the amplification/limitation procedure described above, i.e., B_{sw} is replaced by the smaller of B_{sw} or (60 nT)/f. In this case (Figure 4b), a value f = 8 was found to optimize the fit.

A similar, though less dramatic, improvement resulted from this amplification/limitation procedure in every function tested that depends on B. The results shown below refer in each case to the optimum value of f determined for each function separately; these optimum values of f range between five and eight.

Of the theoretical predictions that were tested, the highest correlation was provided by (2) above [Sonnerup, 1974; Hill, 1975]. The plot of observed versus predicted potential for (2) is shown in Figure 5; the associated correlation coefficient is 0.87. Table 1 shows the parameters of the least-squares regression analysis for this and the other four predictive functions tested (equation (1) above [Hill, 1975], equation (3) of Kan and Lee [1979], equation (21a) of Atkinson [1978], and equation (14) of Gonzales and Mozer [1974]). In the table, a_0 and a_1 are the coefficients of the best-fit straight line

$$\phi = a_0 + a_1 x$$

where ϕ is the observed potential drop and x is the predicted value (e.g., the right-hand side of (1) or (2)). In the case of equations (1) and (2), x is dimensionless (normalized such that $0 \leq x \leq 1$), so that both a_0 and a_1 have units of kV. The parameter r is the linear correlation coefficient and χ^2 is the mean-square deviation of the points from the line, normalized by dividing by $(20\ kV)^2$, the square of the maximum estimated intrinsic uncertainty of the data values. Thus a good fit is represented by $r \approx 1$ or by $\chi^2 \lesssim 1$. The table also shows the optimum field amplification factor f for each fit.

Table 1 shows that (2) reproduces the data

TABLE 1. Parameters of the Least-Squares Fits $\phi = a_0 + a_1 x$

x	a_0	a_1	f	r	χ^2
RHS of (2)	38	122	7	0.87	0.64
RHS of (1)	32	103	7	0.84	0.78
K-L (3)	39	0.014	--	0.75	1.1
Atk (21a)	57	0.032	--	0.53	1.9
G-M (14)	58	0.027	5	0.47	2.3

On the RHS of our equations (2) [Sonnerup, 1974; Hill, 1975] and (1) [Hill, 1975], B_{sw} is multiplied by the amplification factor f and the result is limited to values $B_1 \leq B_2 = 60$ nT (see text). The amplification/limitation procedure is as specified explicitly in equation (3) of Kan and Lee [1979] and equation (21a) of Atkinson [1978]. In equation (14) of Gonzales and Mozer [1974], B_{sw} is multiplied by f and the result is limited as prescribed in that paper.

slightly better than (1), and that both are clearly superior to the other theoretical results tested. The deficiency in the Gonzales and Mozer result lies largely in their scheme for amplification and limitation of |B| (their equation (16)), and the problem with the Atkinson result probably lies partly in the hydrodynamic flow approximation and partly in the use of a limiting case of equation (1) above rather than of the full dependence on B and θ. (Atkinson gives two sets of results, one for small IMF magnitudes and one for large IMF magnitudes; in the test shown here we used his small IMF result for $B_{sw} \leq 5$ nT and his large IMF result for $B_{sw} > 5$ nT. We used his result (21a) derived for a circular merging region; his result (21c) given for a merging region elongated in the east-west direction showed significantly less correlation (r = 0.26) than that shown in Table 1.)

Two general conclusions can be drawn from Table 1. First, the generalized results of magnetic merging theory, as represented by equations (1) or (2), are successful in predicting the variation of the polar cap potential drop within the accuracy to which it can presently be measured (~ 20 kV). Second, a residual potential drop $a_0 \sim 35$ kV (± 10 kV) remains when the merging theory predicts zero, and this residual may logically be attributed to non-merging (closed model) transfer processes. (As we noted in the data analysis section above, the presence of an imbedded reverse convection cell may cause us to overestimate the potential drop by as much as 5 kV and, because such reverse cells are typically associated with northward IMF components, the residual (non-merging) potential drop may have been similarly overestimated.)

We have tested a wide variety of other combinations of interplanetary parameters for their correlation with the polar cap potential drop, motivated primarily by the results of earlier empirical studies. A representative sample of the results is shown in Table 2, which has the same format as Table 1. In general, we note that the solar wind velocity v is totally uncorrelated, the IMF magnitude B is positively, but not highly, correlated, and that any function that emphasizes the southward GSM component of the IMF exhibits a strong positive correlation (with r in the range 0.7 to 0.9). (Recall that in each of these correlations the field strength B is obtained from the amplification/limitation process described above; without this modification the correlation coefficients in Table 2 would be significantly lower, in the range 0.5-0.7)

The Perrault-Akasofu parameter $\varepsilon = vB^2\sin^4(\theta/2)$ provides the highest correlation coefficient (0.89) and the smallest normalized mean-square deviation (0.53) of any of the interplanetary functions tested. Because this function was arrived at empirically (through its correlation with the AE index) rather than theoretically, the significance of this fit is not clear. We note, however, that the 'residual' potential drop $a_0 = 30$ kV is in this case consistent with the values inferred from the fits of (1) and (2) (Table 1). We found that the ε parameter correlates more closely with Φ^2 than with Φ, as suggested by Kan and Lee [1979]; the best fit was $\Phi^2 = 0.93\ \varepsilon - 319$, with f = 7 and r = 0.92.

Although our primary purpose is to investigate the response of the polar cap potential drop to interplanetary conditions, it is also of some interest to search for correlations between the polar cap potential drop and various indices that presumably reflect the magnetospheric and/or ionospheric response to the solar-wind energy input. Of such indices, the AE index was found to have the highest degree of correlation (r = 0.71; $\chi^2 = 1.75$), and the associated coefficients were $a_0 = 41$ kV, $a_1 = 0.11$ kV/nT. By comparison, the Kp index exhibits a relatively weak correlation (r = 0.55, $\chi^2 = 2.1$), presumably because (1) the intrinsic 3-hour time resolution of Kp tends to smear its response to variations in φ, and (2) Kp probably responds also to low-latitude magnetospheric disturbances not directly related to φ [see Heppner, 1977].

Kivelson [1976] has reviewed a number of studies that attempt to deduce the cross-tail

TABLE 2. Parameters of the Least-Squares Fits $\phi = a_o + a_1 x$

x	a_o	a_1	f	r	χ^2
v	74	-0.013	--	0.04	3.0
B	0.12	11	7	0.59	1.9
$-B_z$	62	8.9	7	0.67	1.4
B_s	46	17	7	0.78	1.0
vB_s	45	0.040	5	0.81	0.90
$vB \sin^2(\theta/2)$	7.6	0.038	8	0.81	0.88
$\epsilon = vB^2 \sin^4(\theta/2)$	30	6.1×10^{-3}	8	0.89	0.53

v is in km/s; all B components are in nT and are multiplied by the ratio (60 nT/fB) when that ratio is < 1 (see text).

electric field strength from observations of particle drift boundaries in the magnetospheric equatorial plane, and has listed several Kp-dependent functions that have been derived to represent the response of the tail electric field strength to variations in geomagnetic activity. If the response of the magnetosphere to the imposed polar cap potential drop were simple and linear, one might expect these functions to show a high degree of correlation with the polar cap potential drop. We have found this not to be the case. Of the Kp-dependent functions listed by Kivelson, two (her equations (6) and (18)) are correlated with ϕ only as well as is Kp itself ($r = 0.55$), and the others are even less well correlated ($r \lesssim 0.4$). This lack of correlation is not surprising in view of the known complexity of the magnetotail's response to variations in the solar-wind input.

As a final example, the vorticity area index (VAI) is a meteorological index that has sometimes beeen found to correlate with interplanetary magnetic sector structure, and this correlation is sometimes cited as evidence of a short-term sun/weather effect [e.g., Roberts and Olson, 1973]. We have found the VAI to be totally uncorrelated ($r = 0.03$) with the polar cap potential drop.

Summary and Conclusions

Of many thousands of 'polar' passes of the AE-C and -D satellites, only 32 were found to be suitable for unambiguous determination of the cross polar cap potential drop during a time when simultaneous interplanetary measurements were available. In the future, continuous monitoring by true polar-orbiting satellites and by probes in the upstream solar wind should enable us to develop a reliable scheme for predicting the polar cap potential drop from the parameters of the upstream solar wind. Our results indicate that such a predictive scheme should be feasible.

From our analysis of the limited data set available here, we can draw the following conclusions:

1. The magnetosheath magnetic field strength at the nose of the magnetosphere is evidently amplified by a factor of about 7 to 8 in comparison with the IMF strength as a combined result of bow shock compression and the Zwan-Wolf depletion effect, subject to the limitation that it not exceed the internal geomagnetic field strength. Virtually any formula that utilizes IMF parameters to predict the polar-cap potential drop has improved success when this amplification/limitation process is taken into account.

2. There is strong evidence that dayside magnetic merging is responsible for producing the bulk of the polar cap potential drop, and the variation of the potential drop with interplanetary parameters conforms closely with expectations based on merging theory.

3. A persistent potential drop of about 35 kV ($\pm$ 10 kV) is evidently not attributable to magnetic merging (as presently understood), and may reasonably be attributed to a 'viscous' or 'closed model' process.

4. The polar cap potential drop is apparently related more clearly and directly to interplanetary parameters than to conventional indices of geomagnetic activity. The polar cap potential drop is a direct, linear measure of the strength of the solar wind magnetosphere interaction, but this solar wind input is modified by nonlinear magnetospheric processes before producing the magnetospheric and ionospheric phenomena that are reflected in the geomagnetic indices.

Acknowledgments. Data from the AE-C and AE-D Drift Meter experiments were provided by W. B. Hanson and R. A. Heelis through the Atmosphere Explorer Program central computer at NASA Goddard Space Flight Center. Data from the S3-3 electric field instrument were provided by F. S. Mozer. Interplanetary data were provided by N. F. Ness and others through the World Data Center and the Interplanetary Medium Data Book. We are grateful to all the above individuals and organizations for making a correlative study of this type possible. We thank W. J. Burke, A. J. Dessler, W. B. Hanson, M. Harel, and R. A. Heelis for helpful

comments. This research was supported in part by the Solar-Terrestrial Division of the National Aeronautics and Space Administration (grant NGR44-006-137) and by the Division of Atmospheric Sciences of the National Science Foundation (grants ATM77-12619 and ATM80-17316).

The Editor thanks J. R. Kan and J. L. Burch for their assistance in evaluating this paper.

References

Arnoldy, R. L., Signature in the interplanetary medium for substorms, J. Geophys. Res., 76, 5189, 1971.

Atkinson, G., Energy flow and closure of current systems in the magnetosphere, J. Geophys. Res., 83, 1089, 1978.

Axford, W. I., and C. O. Hines, A unifying theory of high-latitude geophysical phenomena and geomagnetic storms, Can. J. Phys., 39, 1433, 1961.

Banks, P. M., J.-P. St. Maurice, R. A. Heelis, and W. B. Hanson, Electric fields and electrostatic potentials in the high latitude ionosphere, in Exploration of the Polar Upper Atmosphere, edited by J. Holtet and C. S. Deehr, D. Reidel, in press, 1981.

Burch, J. L., Rate of erosion of dayside magnetic flux based on a quantitative study of the dependence of polar cusp latitude on the interplanetary magnetic field, Radio Sci., 8, 955, 1973.

Burch, J. L., Observations of interactions between interplanetary and geomagnetic fields, Rev. Geophys. Space Phys., 12, 363, 1974.

Burke, W. J., M. C. Kelley, R. C. Sagalyn, M. Smiddy, and S. T. Lai, Polar cap electric field structures with a northward interplanetary magnetic field, Geophys. Res. Lett., 6, 21, 1979.

Caan, M. N., R. L. McPherron, and C. T. Russell, Substorm and interplanetary magnetic field effects on the geomagnetic tail lobes, J. Geophys. Res., 80, 191, 1975.

Cowley, S. W. H., Comments on the merging of nonantiparallel magnetic fields, J. Geophys. Res., 81, 3455, 1976.

Cowley, S. W. H., Magnetospheric asymmetries associated with the Y-component of the IMF, Planet. Space Sci., 29, 79, 1981.

Crooker, N. U., Explorer 33 entry layer observations, J. Geophys. Res., 82, 515, 1977.

Crooker, N. U., Dayside merging and cusp geometry, J. Geophys. Res., 84, 951, 1979.

Dungey, J. W., Interplanetary magnetic field and the auroral zones, Phys. Rev. Lett., 6, 47, 1961.

Eviatar, A., and R. A. Wolf, Transfer processes in the magnetopause, J. Geophys. Res., 73, 5561, 1968.

Feldstein, Y. I., Auroral oval, J. Geophys. Res., 78, 1210, 1973.

Foster, J. C., D. H. Fairfield, K. W. Ogilvie, and T. J. Rosenberg, Relationship of interplanetary parameters and occurrence of magnetospheric substorms, J. Geophys. Res., 76, 6971, 1971.

Garrett, H. B., A. J. Dessler, and T. W. Hill, Influence of solar-wind variability on geomagnetic activity, J. Geophys. Res., 79, 4603, 1974.

Gonzales, W. D., and F. S. Mozer, A quantitative model for the potential resulting from reconnection with an arbitrary interplanetary magnetic field, J. Geophys. Res., 79, 4186, 1974.

Hanson, W. B., D. R. Zuccaro, C. R. Lippincott, and S. Sanatani, The retarding-potential analyzer on Atmosphere Explorer, Radio Sci., 8, 333, 1973.

Harel, M., R. A. Wolf, P. H. Reiff, R. W. Spiro, W. J. Burke, F. J. Rich, and M. Smiddy, Quantitative simulation of a magnetospheric substorm, 1, Model logic and overview, J. Geophys. Res., 86, 2217, 1981.

Heppner, J. P., Polar cap electric field distributions related to the interplanetary magnetic field direction, J. Geophys. Res., 77, 4877, 1972.

Heppner, J. P., Empirical models of high-latitude electric fields, J. Geophys. Res., 82, 1115, 1977

Hill, T. W., Magnetic merging in a collisionless plasma, J. Geophys. Res., 80, 4689, 1975.

Hill, T. W., Generation of the magnetospheric electric field, in Quantitative Modeling of Magnetospheric Processes, Geophysical Monogr. Ser., vol. 21, edited by W. P. Olson, p. 297, Amer. Geophys. Union, Washington, D. C., 1979.

Hill, T. W., and R. A. Wolf, Solar-wind interactions, in The Upper Atmosphere and Magnetosphere, edited by F. S. Johnson, p. 25, National Academy of Science, Washington, D. C., 1977.

Johnson, F. S., The driving force for magnetospheric convection, Rev. Geophys. Space Phys., 16, 161, 1978.

Kan, J. R., and L. C. Lee, Energy coupling function and solar-wind magnetosphere dynamo, Geophys. Res. Lett., 6, 577, 1979.

King, J. H., Interplanetary Medium Data Book--Supplement 1, National Space Science Data Center, Greenbelt, Md., 1979.

Kivelson, M. G., Magnetospheric electric fields and their variation with geomagnetic activity, Rev. Geophys. Space Phys., 14, 189, 1976.

Meng, C.-I., R. H. Holzworth, and S.-I. Akasofu, Auroral circle--delineating the poleward boundary of the quiet auroral belt, J. Geophys. Res., 82, 164, 1977.

Murayama, T., and K. Hakamada, Effects of solar wind parameters on the development of magnetospheric substorms, Planet. Space Sci., 23, 75, 1975.

Perrault, P., and S.-I. Akasofu, A study of geomagnetic storms, Geophys. J. R. Astron. Soc., 54, 547, 1978.

Petschek, H. E., The mechanism for reconnection of geomagnetic and interplanetary field lines, in The Solar Wind, edited by R. J. Mackin, Jr. and M. Neugebauer, p. 257, Pergamon, New York, 1966.

Reiff, P. H., R. W. Spiro, and T. W. Hill, Prediction of the polar cap potential drop, in High Latitude Electric Fields in the Magnetosphere and Ionosphere, edited G. S. Stiles and F. T. Berkey, p. 22-1, AGU, Washington, D. C., 1979.

Roberts, W. O., and R. H. Olson, New evidence for effects of variable solar corpuscular emission on the weather, Rev. Geophys. Space Phys., 11, 731, 1973.

Rostoker, G., H.-L. Lam, and W. D. Hume, Response time of the magnetosphere to the interplanetary electric field, Can. J. Phys., 5, 544, 1972.

Russell, C. T., and G. Atkinson, Comments on a

paper by J. P. Heppner, 'polar cap electric field distributions related to interplanetary magnetic field direction', J. Geophys. Res., 78, 4001, 1973.
Russell, C. T. and R. L. McPherron, Semiannual variation of geomagnetic activity, J. Geophys. Res., 78, 7490, 1973.
Sonnerup, B. U. O., Magnetopause reconnection rate, J. Geophys. Res., 79, 1546, 1974.
Spiro, R. W., P. H. Reiff, J. L. Burch, and R. A. Heelis, High latitude plasma convection and the IMF (abstract), EOS Trans. AGU, 60, 915, 1979.
Spreiter, J. R., and A. Y. Alksne, Plasma flow around the magnetosphere, Rev. Geophys., 7, 11, 1969.
Stern, D. P., Large-scale electric fields in the earth's magnetosphere, Rev. Geophys. Space Phys., 15, 156, 1977.
Vasyliunas, V. M., Theoretical models of magnetic field line merging, Rev. Geophys. Space Phys., 13, 303, 1975.
Wolf, R. A., Effects of ionospheric conductivity on convective flow of plasma in the magnetosphere, J. Geophys. Res., 75, 4677, 1970.
Zwan, B. J., and R. A. Wolf, Depletion of solar-wind plasma near a planetary boundary, J. Geophys. Res., 81, 1636, 1976.

(Received February 3, 1981;
revised June 19, 1981;
accepted June 25, 1981.)